Monitoring of Dose Dependent Damage in MeV Energy Hydrogen Implanted Silicon by Photo-Modulated Reflectance Measurements

J. SZÍVÓS[1], L. BALOGH[1], I. RAJTA[2], G. U. L. NAGY [iD][2], Z. T. GAÁL[2], V. SAMU[1], K. TAKEFUMI[3], AND Z. ZOLNAI [iD][1]

1 Semilab Semiconductor Physics Laboratory Ltd., 1117 Budapest, Hungary
2 Tandetron Laboratory, Institute for Nuclear Research (ATOMKI), 4026 Debrecen, Hungary
3 Semilab Japan KK, Kanagawa 222-0033, Japan

CORRESPONDING AUTHOR: J. SZÍVÓS (e-mail: janos.szivos@semilab.hu)

ABSTRACT High-energy low-mass proton implantation achieved considerable interest in semiconductor technology, due to much deeper penetration of hydrogen ions into silicon as compared to common dopants, boron, phosphorous, and arsenic. Accordingly, monitoring the accumulation kinetics and stability of proton-implantation induced defects and their influence on the optical and electrical properties of Si achieved increased attention both in technological process control and scientific research. We show that photo-modulated-reflectance (PMR) is effective technique to measure very low defect concentrations in the ppb-ppm range in high energy proton implanted silicon. After ion irradiation, the as-implanted dilute damage structure may lead to long term changes of the defect distribution and the formation of defect compounds due to mobility of point defects at room temperature. Moreover, low-mass hydrogen atoms may move significantly faster at room temperature compared to heavier dopants. We show that PMR is capable to detect differences in implanted proton dose with high sensitivity in a wide dose range, and, on a longer time scale, allows to follow changes in free carrier generation and recombination processes through the measurement of the long term decay of the PMR signal which is related to the sample response based on electro-optic and thermo-optic effects. Our experiments may pave the way toward high precision process control of device structure fabrication which utilizes the high-energy hydrogen implantation step. Also, our aim is to gain insight into the main processes underlying the dose dependent change and long-term decay of the PMR signal in high energy proton implanted Si.

INDEX TERMS Silicon, hydrogen implantation, defect concentration, photo-modulated-reflectance (PMR), decay process.

I. INTRODUCTION

Ion implantation is one of the most common processes utilized in semiconductor manufacturing. Nevertheless, the implantation depth for common dopants is limited due to the mass of B^+, P^+, or As^+. Irradiation of light mass ions like protons go beyond this limit and can be utilized to adjust the doping of silicon power devices even in deep substrate regions. Proton implantation into silicon is applied for several purposes. Low dose implantations can be applied in power electronic devices to fine tune the charge carrier lifetime, improving the switching properties [1], [2], while medium dose proton implants generate hydrogen related donor states and are used for creating n-type buried regions or deep wells in the semiconductor material [3]. High-energy, low-mass hydrogen ions generate several orders of magnitude lower defect concentrations as compared to the heavier B^+, P^+, or As^+ implants, due to their low nuclear stopping cross-section for silicon atomic nuclei and deep penetration to several tens of microns. Defect-related implantation dose monitoring for MeV-energy proton implants requires non-destructive high sensitivity characterization techniques for technology control. Besides precise monitoring of very low damage levels,

the relaxation and reconfiguration of the dilute defect structure on a longer time scale after the implantation process is important task. Also, changes in the depth distribution of hydrogen, its interaction with defects, and hydrogen impurity related resistivity changes in the material [2], are of great interest in technology control, industrial applications [2], and materials science.

To date the Photo-modulated-reflectance (PMR) technique has been successfully applied for doping concentration monitoring and shallow junction depth profiling in silicon [4]. Also, detailed description and modeling of the PMR process has been presented [5]. However, less attention was paid to the analysis of the PMR signal detected from ion implantation damaged un-annealed silicon layers with excess defect related recombination centers introduced by the irradiation process.

In this work, we show that the photo-modulated reflectance technique enables high-sensitivity damage and thus dose monitoring for 600 keV and 1.5 MeV hydrogen implants from low to medium dose range, and, in addition, enables to follow post-implantation changes in the sample structure on a longer time scale. This is thank to the large penetration and information depth of PMR in slightly damaged Si ($\sim$10 μm for the pump and $\sim$50 μm for the probe laser beam) as well as its extreme sensitivity on sample reflectance changes which are due to the variation of the free carrier concentrations and lifetimes depending on damage concentration and the actual defect structure.

Previous works revealed significant dependence of free carrier lifetimes for 1.5 MeV H-implanted Si for a studied dose range of 10^{11}–10^{14} H$^+$ cm^{-2} [6], [7]. As the PMR response is closely related to the lifetime of photo-induced carriers, tiny changes in damage levels and/or the hydrogen depth distributions are expected to appear in the PMR signal. Therefore, PMR can be anticipated as a very sensitive technique to monitor differences in the implantation dose for deep proton implants.

Room temperature micro-photoluminescence (μ-PL) imaging measurements were also performed on our hydrogen implanted samples. Differences in residual damage levels vs. implantation dose were monitored via the intensity of the band-to-band (B2B) PL lines to gain additional information for free carrier generation and recombination processes in slightly damaged silicon.

Note our preliminary results were published elsewhere [8].

II. EXPERIMENTAL

A. SAMPLES

A high purity bare, <100> Si wafer with diameter of 300 mm was exposed to 1.5 MeV energy H$^+$ ion-beam treatments. The sample (purchased from SUMCO Corp.) is p-type, B-doped with resistivity of 20-30 Ωcm and corresponding doping concentration of $\sim$10^{15} cm^{-3}. 600 keV proton implants were performed on a 200 mm diameter <100> Si wafer.

B. METHODS

In the case of H implants the time interval between the implantation process and the characterization step is a crucial parameter due to the fast self-decay and the long term diffusion and/or complex defect formation tendency of single defects and hydrogen atoms. To lower time delay between implantation and measurement, the ion irradiation was performed by our closest available partner, the Tandetron Laboratory of the Institute for Nuclear Research (ATOMKI) in Debrecen, Hungary [9].

The ion implantation process has been realized by exposing the sample to the H$^+$ beamline of the Tandetron ion accelerator [8]. The irradiation took place in air for 1.5 MeV protons and in vacuum (about 10^{-5} Pa) for 600 keV protons. The ion beam in air had circular shape with a maximum diameter of ca. 4.5 mm and nearly homogeneous ion flux distribution. In vacuum, the beam was collimated using a 2mm $\times$ 2mm aperture and the ions lateral density was measured to be homogeneous. For all implants the sample was scanned with constant velocity in front of the incident beam. In this manner, spatially quasi-homogeneous stripes of different doses could be obtained depending on the scanning velocity and beam current. For the in air irradiations the exit window at the end of the beamline was a Ti foil, and the sample-window distance was kept at 5 mm. This gap may be wide enough to homogenize the beam intensity profile, and, at the same time, is narrow enough to keep the energy loss of the beam in air below $\sim$6% with respect to the nominal energy. In all cases, the tilt angle between the sample normal and the beam was set to 7$°$ in order to avoid ion channeling effects.

For 1.5 MeV implants five stripes with 80 mm width and 4.5 mm height of highly different doses (10^{11}, 10^{12}, 10^{13}, 10^{14}, and 10^{15} H$^+$ cm^{-2}) were prepared by the above-mentioned irradiation procedure while keeping a vertical spacing of 10 mm between the centers of neighboring stripes. For in vacuum implants (600 keV and 1.5 MeV) three stripes with 6 mm width and 2 mm height of slightly different doses (1.8×10^{14}, 2×10^{14}, and 2.2×10^{14} H$^+$ cm^{-2}) were prepared with a vertical spacing of 5 mm between the midlines of neighboring stripes. The applied nominal doses are listed also in Table 1.

PMR experiments have been carried out with a Semilab PMR-3000S tool, while μ-PL measurements were performed using a Semilab En-Vision system in the band-to-band (B2B) PL detection wavelength range of 1000-1300 nm, and at excitation wavelength of $\lambda = 808$ nm.

C. SAMPLE PREPARATION

The implanted stripes were prepared one after the other starting with the highest implanted dose. Furthermore, ca. 2.5 hours is required for sample transport from the Tandetron Lab of ATOMKI in Debrecen to the PMR tool located at Semilab headquarters in Budapest. Due to these conditions, the time delay between the implantation and the first PMR

TABLE 1. Sample parameters.

H+ energy	Dose (H+/cm²)	Time delay	PMR decay fit data		
1.5 MeV	10¹⁵	4 months			
	10¹⁴				
	10¹³				
	10¹²				
	10¹¹				
			P_0	P_D	t_D (h)
600 keV	2.2×10¹⁴	8:40 (h:min)	771	52	24,6
	2×10¹⁴	7:35 (h:min)	746	58	22.7
	1.8×10¹⁴	8:05 (h:min)	716	57	22.8
			$N_{def,0}$ (cm⁻³)	$N_{def,D}$ (cm⁻³)	t_D (h)
	2×10¹⁴	7:35 (h:min)	6.2E15	4.5E14	22.4
			ΔN_0 (cm⁻³)	ΔN_D (cm⁻³)	t_D (h)
			2.9E18	1.5E17	22.5

H+ ion energy, nominal dose, and time delay between implantation and the first PMR measurement for the implanted stripes. Exponential decay fit parameters for 600 keV+ energy implants are also shown.
Note $y(t) = y_0 + y_D \exp(-t/t_D)$, where $y = P$ or N_{def}, i.e., PMR signal or defect concentration, and t_D is time constant.
For excess carrier concentration $\Delta N(t) = \Delta N_0 + \Delta N_D(1 - \exp(-t/t_D))$ applies.

measurement is relatively long and it's different for each implanted stripe (see Table 1).

For the 600 keV implants the PMR analysis (following the decay of the PMR signal vs. time for different implanted doses) has been carried out as following. All the implanted stripes were crossed through in one measurement run to keep nearly similar delays for the different dose implants.

After the first run the laser beam of the PMR tool was positioned again on the first stripe but on a new fresh area and a second PMR run was started through all the stripes. The whole measurement procedure was repeated several times until the decay process has been nearly saturated. For 1.5 MeV implants one measurement run through the stripes was performed long time (4 months) after the saturation of the decay process.

En-Vision B2B PL measurements were performed on 1.5 MeV H+ implanted samples relatively long time (saturation of decay) after the ion implantation process.

III. RESULTS AND DISCUSSION
A. COMPUTER SIMULATION OF DAMAGE DISTRIBUTION
The simulations of 600 keV and 1.5 MeV hydrogen implantation induced damage vs. depth in Si have been performed with full-cascade SRIM [10] calculations. The results can be seen in Fig. 1, where damage is shown in units of displacements per atoms (dpa). SRIM calculates the number of vacancies per impinging ion and unit depth (vacancies/(ion×Angström)), remaining after collision cascade processes came to rest. This quantity can be converted
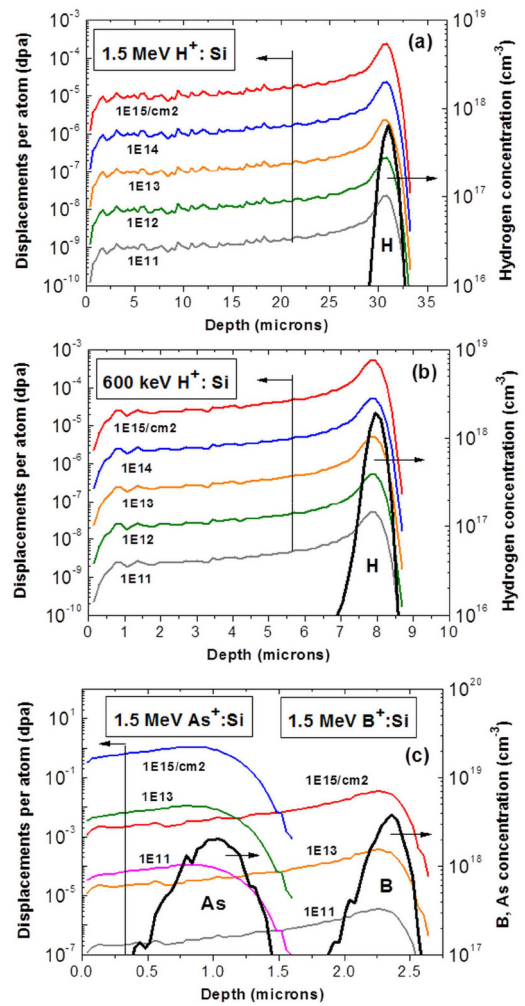

FIGURE 1. Depth distributions of (a) 1.5 MeV and (b) 600 keV energy proton implantation induced damage in Si resulted by full-cascade SRIM [10] simulations. Thick black lines show hydrogen depth profiles for a dose of 10¹⁴ H+/cm². (c) SRIM depth distributions of 1.5 MeV energy B+ and As+ implantation induced damage in Si. Thick black lines show boron and arsenic depth profiles for a dose of 10¹⁴/cm².

to *dpa* units multiplying by $C_a \times 10^8$ and by the ion dose (ions/cm²) and dividing by the atomic density of Si (N_{Si} = 5×10²²/cm³). Note, SRIM vacancy distributions were corrected with a defect accumulation (defect endurance) factor [11] of $C_a = 0.1$ that has been determined from Crystal-TRIM simulations of implantation into Si with relatively low-mass boron ions [10]. In literature we did not find specific defect endurance parameter for proton implantation, therefore the C_a value of the light boron projectile was applied. For the defect endurance corrected vacancy concentration (N_{vac}) it follows: $N_{vac} = dpa \times N_{Si}$.

Low-mass protons with 1.5 MeV energy introduce very low damage levels, between 10^{-5} and 10^{-9} dpa, for the applied dose range in the uppermost ~32 µm of Si, and even the damage peak (located at a depth of about 30 µm) for the highest dose applied is below 10^{-3} dpa.

Compared to 1.5 MeV protons, for 600 keV protons about three times higher damage levels are introduced in the

uppermost 8 μm of Si, such difference is due to the higher collision cross-section at lower implant energy. Thick black lines in Fig. 1 show SRIM simulated hydrogen depth distributions for a dose of 10^{14} H$^+$ cm^{-2}. Most of the implanted hydrogen atoms are concentrated at the maximum penetration depth. The atomic peak concentration of implanted hydrogen varies between $\sim 10^{15}$ cm^{-3} and $\sim 10^{19}$ cm^{-3} in the applied dose range. Note SRIM damage profiles scale linearly with implanted dose as dynamic defect recombination and in-situ local annealing processes cannot be taken into account in the SRIM simulation (C_a modifies only the proportionality factor between vacancy concentration and dose).

Fig. 1(c) shows SRIM simulated damage distributions in Si for 1.5 MeV B$^+$ and As$^+$ implantation in the dose range 10^{11}-10^{15} cm^{-2} for comparison. B and As atomic concentrations are also plotted for a dose of 10^{14} cm^{-2}. For B and As two and five orders of magnitude higher damage levels can be observed as compared to that for 1.5 MeV hydrogen implants. The highest dose As$^+$ implant leads to amorphization of Si.

B. PMR SIGNAL EVALUATION

In our simplified model we consider the high energy proton implanted sample as nearly homogeneously damaged Si crystal within the ion penetration range. This seems to be reasonable looking at the SRIM depth profiles in Fig. 1. In first approximation we neglect gradients at the surface as possible source of excess recombination and do not consider gradients and extra carrier capture at the deeply buried ion projected range (we expect negligible PMR signal contribution from this region). Since defect levels are very low we consider similar laser induced excess (hot) carrier generation rates in bare and implanted Si. For excess carrier recombination at implantation induced defects similar effective cross section was supposed for all individual capture centers introduced into single crystalline Si.

In our PMR experiment the sample is exposed to a pump laser beam ($\lambda = 808$ nm) of which power is modulated with a relatively low frequency ($f_{mod} = 2$ kHz) AC component. Such pump laser power modulation in the implanted sample leads to quasi-static periodic generation of excess carriers, electrons and holes, with maximum concentration change ΔN and ΔP, and accordingly, modulation of the refractive index n by a maximum change Δn. This Δn change is detected through the relative reflectance change $\Delta R/R_0$ of the sample, which is measured through the sample-induced AC modulation (at frequency $f = f_{mod}$) in the reflected power of the initially unmodulated (DC) probe laser beam ($\lambda = 980$ nm). Note that the phase of the periodical reflectance change (material response) may differ from that of the pump laser (AC) modulation. Since the modulation frequency is low compared to the plasma frequency, a quasi-static response is generated where this phase shift can be $\sim 0°$ or $\sim 180°$ indicating the sign of $\Delta R/R_0$. The relation between ΔN, ΔP and ΔR for homogeneous defect depth

distribution (considering an average effective defect concentration in the implanted layer) can be given by the following expression [5]:

$$\Delta R/R_0 = |4/\left(1 - n^2\right)|\left\{\beta\left(\Delta N/m_e * + \Delta P/m_h *\right) + \delta_T \Delta T\right\}$$
(1)

where n = 3.58, R_0 = 0.317, and $\beta = -1.2 \times 10^{-22}$ are refractive index, sample reflectance, and electro-optic coefficients of Si, respectively, at the probe laser frequency [12], [13]. Furthermore, m_e* and m_h* are the effective mass of electrons and holes, respectively, while ΔT is the temperature increase due to the laser beam. Negative sign of β causes decrease of the refractive index n and the reflectance R for excess carrier concentrations ΔN and ΔP.

Under the steady-periodic pump power modulation condition the formula:

$$G\tau_{tot}(\Delta N) = \Delta N$$
(2)

gives relation between the pump laser induced carrier generation rate (G), full carrier lifetime $\tau_{tot}(\Delta N)$ and the excess carrier concentration ΔN. The full lifetime of excess carriers can be calculated as:

$$\tau_{tot} = \left(\tau_{Aug}^{-1} + \tau_{def}^{-1} + \tau_{ad}^{-1}\right)^{-1}$$
(3)

with the Auger recombination (τ_{Aug}) and defect related (τ_{def}) carrier recombination lifetimes, and lateral ambipolar diffusion-related carrier concentration loss (τ_{ad}) determined by the ambipolar diffusion coefficient D_{ad}. As it was shown, for high ΔN values the Shockley-Read-Hall recombination rate can be neglected [5]. We computed G, τ_{Aug} and D_{ad} according to [5], [12]. The high power density of the generation laser ($I_{las} = 5.6 \times 10^5$ W cm^{-2}) leads to high ΔN values in the $\sim 10^{18}$ cm^{-3} range and in this case $\Delta N = \Delta P$ can be considered, i.e., the low doping of the Si wafer can be neglected with respect to ΔN and ΔP.

Extracted values of τ_{def} allow the estimation of defect concentrations N_{def} via $\tau_{def} = 1/(\sigma_d v_{th} N_{def})$, where σ_d and v_{th} are recombination cross section of defects, and thermal velocity of electrons, respectively. Considering typical cross section values for vacancy and hydrogen related defects in Si [14]–[16] we assumed an average defect related capture cross section $\sigma_d = 3 \times 10^{-15}$ cm^{-2}.

In Eq. (1) $\delta_T = 2.9 \times 10^{-4}$ K^{-1} is the thermo-optic coefficient for Si [17] at the probe laser frequency, and it accounts for pump laser induced periodic temperature increase with maximum ΔT in the sample due to phonon-assisted thermal relaxation and recombination processes of the generated (hot) excess carriers [5]. Temperature rise leads to increase of the refractive index n via the thermo-optic effect, and therefore, electro-optic and thermo-optic processes oppositely affect the sample reflectance.

To estimate ΔT for bare Si the following formula can be applied:

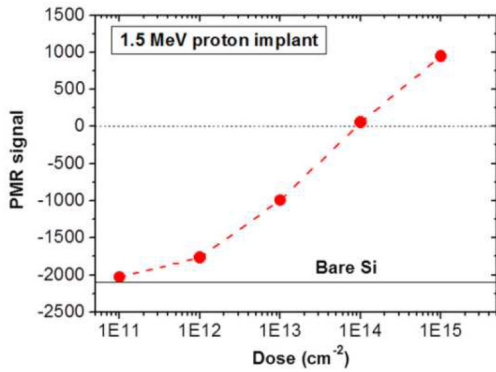$$\Delta T = (H_{hc} + H_{rec})\tau_{td}/\rho C$$
(4)

FIGURE 2. PMR signal for Si implanted by 1.5 MeV protons to different ion doses; red dashed line is only to guide the eye. Solid line marks signal level for un-implanted bare Si, dotted line shows zero PMR signal position. Measurements were carried out 4 months after the ion implantation process.

FIGURE 3. Concentration of defects (dots) and pump laser generated excess carriers (squares) evaluated from PMR measurements as a function of implantation dose. The sample was irradiated with 1.5 MeV protons. Triangle shows the ΔN value for unimplanted bare Si. Dashed line for squares shows linear fit to ΔN on logarithmic dose scale for doses $\geq 1 \times 10^{12}$ H$^+$/cm^2. Dashed line for dots shows linear fit to N_{def} on log-log scale for doses $\geq 1 \times 10^{12}$ H$^+$/cm^2.

where H_{hc} and H_{rec} are hot-carrier heat generation and recombination related heat generation terms, respectively [5], ρ and C are density and heat capacitance of Si, while τ_{td} accounts for the effective time coefficient of thermal diffusion with diffusivity D_{th}.

Our PMR signal value is defined as $10^6 \times \Delta R/R_0$, therefore knowledge on carrier generation/recombination processes allows to derive excess carrier concentrations ΔN and ΔP from the PMR signal by putting together Eqs. (1)-(4). Note more details on the PMR evaluation procedure will be given in a forthcoming paper.

C. RESULTS OF PMR MEASUREMENTS

Fig. 2 shows PMR signal values measured for 1.5 MeV H$^+$ implanted Si. In this case we followed the PMR signal trend in a wide dose range from 10^{11} H$^+$ cm^{-2} up to 10^{15} H$^+$ cm^{-2}. These measurements were performed long time after ion irradiation (see Table 1), therefore in this case PMR decay processes were expected to be fully saturated. For bare Si we obtained a PMR signal of -2095 ± 20, see the solid horizontal line in Fig. 2. For this value an excess carrier concentration $\Delta N = \Delta P = 1.05\times10^{19}$ cm^{-3} can be derived which is indeed significantly higher than the acceptor doping of the Si wafer, i.e., $\sim10^{15}$ cm^{-3}. Ion irradiation introduces defect related capture centers which enhance carrier recombination (heat generation), and lowers free carrier concentration. Such processes affect the net reflectance change so that the PMR signal of the damaged sample will shift from that of undamaged Si. As Fig. 2 shows this shift is monotonous with proton dose and is apparent already for the lowest dose of 10^{11} cm^{-2}. The PMR signal crosses the zero value at a dose of $\sim10^{14}$ H$^+$ cm^{-2}. The zero PMR value means that the contribution of the generated excess carrier concentration, ΔN, to the reflectivity change, i.e., the PMR signal just cancels that of the thermo-optic term (note in Eq. (1) β has negative while δ_T has positive sign). Negative sign of the PMR value below this dose means that the electro-optic term (excess carriers) of the PMR signal is greater than
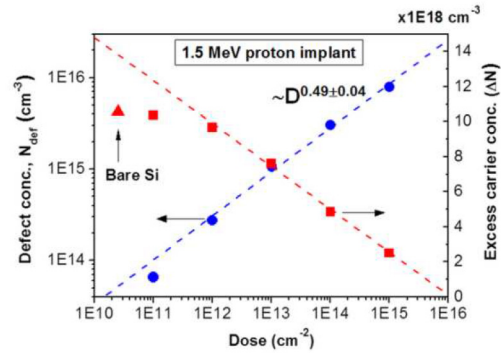
the thermo-optic term (temperature change), while for positive PMR values above this dose, the relation between the two terms turns to opposite. Note the monotonous dependence of the PMR signal on various implantation parameters is utilized in several applications. Besides PMR's dose monitoring capability, we presented the excellent sensitivity of this non-destructive technique for implantation tilt angle and ion beam current density [18]–[20]. It is to mention that the PMR tool has a high spatial resolution as well: it is suitable to measure up to a test pad size of 30 µm × 30 µm, while the beam diameter is around 3 µm.

Fig. 3 shows PMR pump laser induced excess carrier concentration, ΔN, and implantation induced Si defect concentration, N_{def}, vs. dose, for 1.5 MeV proton implants. The linear trend of squares for doses $>10^{11}$ H$^+$cm^{-2} implies inverse logarithmic dose dependence for ΔN, see the red dashed line. Despite the wide dose range applied, change in ΔN is relatively slow and covers roughly an order of magnitude. Our derived τ_{def} value of $\approx1.1\times10^{-8}$ s at 10^{14} cm^{-2} dose is close to that found by another group ($\tau \approx1.5\times10^{-8}$ s) in the upper 10-15 µm thick region of 1.5 MeV, 10^{14} cm^{-2} implanted Si [6] using MW-PCD based carrier decay lifetime depth profiling technique.

Interesting to note that in Fig. 3 N_{def} shows a dose (D) dependence of $\sim D^{0.5}$ instead of a linear defect accumulation vs. dose, see the blue dashed line fitted to dots. The square root dependence can be associated with sub-linear defect accumulation kinetics vs. dose due to effective in-situ defect recombination during ion implantation. For 1.5 MeV H$^+$ implanted Si another group reported an inverse square root dependence of the carrier lifetime vs. dose [6] that also indicates square root dose dependence for the defect concentration. From these results it seems that PMR can be considered as powerful tool to ascertain defect accumulation kinetics for MeV energy light-mass proton implants.

We emphasize that the damage levels for the applied dose values fall in the ppb–ppm range, according to our evaluation
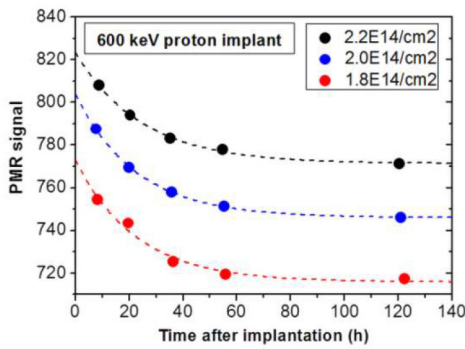
FIGURE 4. Time evolution of the PMR signal for Si implanted by 600 keV protons to different ion doses. Dashed lines represent best fits for exponential decay.

FIGURE 5. Concentration of defects (dots) and pump laser generated excess carriers (squares) evaluated from PMR decay measurements as a function of delay time after the implantation process. The sample is irradiated with 600 keV protons to a dose of 2×10^{14} H$^+$/cm^2. Dashed lines show exponential decay (for dots) and saturated exponential increase (for squares) function fits to data.

of the PMR data. Such defect concentrations are several orders of magnitude lower than those usually generated by higher mass implants, like B$^+$, P$^+$, or As$^+$ in a similar dose range (see Fig. 1). The applicability of PMR to monitor tiny damage fractions is due to its extreme sensitivity to excess carrier concentrations and lifetimes, parameters which are closely related to refractive index changes in the photo-excited material.

Fig. 4 shows PMR values for 600 keV H$^+$ implanted samples measured from ∼8 up to ∼122 hours delay after ion irradiation. In this experiment our aim was to follow the decay characteristics of the PMR signal as well as to check the dose sensitivity of PMR as a function of delay time using samples with slightly different implanted doses of 1.8×10^{14}, 2×10^{14}, and 2.2×10^{14} H$^+$cm^{-2}.

Fig. 4 reveals the high sensitivity of PMR for the H$^+$ dose and shows quite similar long term dependences for the three samples. The 20% difference between the highest and lowest dose is reflected in a PMR signal difference of 6.7% and 7% for the shortest (8 hours) and longest (122 hours) time delays. Nevertheless the PMR signal within the measured timeframe decays by 4.5% (lowest), 5.3% (mid), and 5% (highest dose). The decay seems to be almost completely saturated for the longest delays.

Dashed lines in Fig. 4 show best fits to measured data by an exponential decay function $P(t) = P_0 + P_D \exp(-t/t_D)$. Here t is delay time, t_D is characteristic decay time, while P_0 and P_D are asymptotic value and decay amplitude of the PMR signal. Fitted parameters are summarized in Table 1. For the three samples an average decay time $t_D \approx 23.4 \pm 1$ hours was found. Decay amplitudes are quite similar, however, 10% lower P_D value is found for the highest dose, which is accompanied by a 10% longer time constant, t_D. The results suggest that a long-term physical process in damaged Si may be responsible for PMR signal decay.

As it was mentioned in Section III-A, about three times higher damage levels are predicted by SRIM for the 600 keV energy implants compared to the 1.5 MeV energy ones for same dose values. Fig. 4 shows a PMR signal value of about 750 for 600 keV proton implantation with a dose
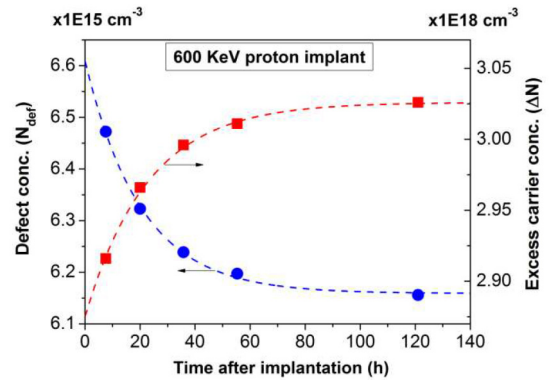
of 2×10^{14} H$^+$cm^{-2} after the saturation of the PMR decay process. On the other hand, extrapolating the PMR signal trend shown in Fig. 2 for 1.5 MeV energy implantation, a PMR value of 750 corresponds to a dose of about 6×10^{14} H$^+$cm^{-2}. Therefore, a dose ratio of about three for the two implantation energies can be ascertained in order to detect a similar PMR signal value. This is in good agreement with the damage ratio predicted by SRIM simulations. Therefore, the PMR data measured for 600 keV and 1.5 MeV implantations seem to follow the expected trend.

In Fig. 5 derived PMR induced excess carrier and Si defect concentrations are shown vs. time for the 600 keV, 2×10^{14} H$^+$cm^{-2} implanted sample. The observed trends are just opposite as ΔN increases while N$_{def}$ decreases, and both of them shows exponential character with quite similar time constants of $t_D \approx 22.5 \pm 1$ hours, being close to t_D of the PMR value (22.7 ± 1 hours). From Table 1 it follows that the overall drop of N$_{def}$ is about 7%, and the full increase of ΔN is about 5%, however, the magnitudes of their asymptotic values differ by nearly three orders. The evaluated average defect concentration is ∼6×10^{15} cm^{-3}, much lower than predicted by corrected SRIM simulations (for the concentration of vacancies: N$_{vac} > 10^{17}$ cm^{-3}), see Fig. 1(b). This also suggests significant in-situ defect reduction during implantation, i.e., before the start of the slower post-implantation defect relaxation process detected by the PMR decay on longer time scale.

For interpretation of the PMR decay process one may consider the followings. A high mobility defect in Si is the isolated vacancy (V$_{Si}$). To date, a number of extensive studies report on vacancy migration in silicon both at cryogenic and elevated temperatures [21]–[23]. The diffusion coefficient of V$_{Si}$ was found to be D$_V$ $= (0.0012$ cm^{2}s$^{-1}) \times \exp(-0.45\text{eV}/kT)$ [21], where k is Boltzmann constant and T is temperature. Based on this, for room temperature (RT) and a duration of $t = 24$ hours a diffusion length of $(D_V t)^{1/2} \approx 12$ μm can be derived,

which is comparable to the maximum penetration depth of 600 keV H^+ ions, see Fig. 1(b). Nevertheless, in irradiated material, depending on the defect structure, only a fraction of vacancies can freely migrate toward the bulk or the surface since they can be captured by another defects or dopant atoms in the damaged region to form defect complexes of low thermal mobility and ability to capture free carriers.

Previously, in electron irradiated Si samples a diluted defect structure has been found beneath the sample surface after irradiation, i.e., the concentration of V_{Si} related defects such as divacancies (VV), vacancy-oxygen (VO) pairs, and vacancy-phosphorus (VP) pairs, has shown exponential like decay toward the sample surface in the uppermost 3-6 µm of the damaged layer [23]. This result was attributed to the migration of V_{Si} in the irradiated material. In another work, carrier decay lifetime profile measurements in 1.5 MeV proton implanted Si revealed a continuous decrease of carrier lifetime (τ_R) from the position of the H^+ projected range toward the sample surface, starting with τ_R ~0.5 µs at the substrate side and descending to τ_R ~15 ns in the near surface region [6]. On the other hand, smooth primary damage profiles without significant gradients in a wide depth range below the surface can be expected for high-energy as-implanted Si, see Fig. 1. From the experiments mentioned above partial reorganization of the defect structure at RT after (and during) ion irradiation can be inferred for high energy proton implants. Underlying mechanisms may be redistribution of mobile vacancies and/or hydrogen atoms, e.g., gettering and recombination at the surface [23] and complex defect formation with the participation of vacancies, dopant atoms, or hydrogen.

Concerning the migration of hydrogen in ion implanted Si the reported diffusion constants vary over six orders of magnitude [24]. This wide spread of data is caused by the different concentrations of defects in the studied samples. Hydrogen diffusion is slowed down as it interacts with impurities. In a comprehensive work, for RT an effective diffusion coefficient of ~10^{-12} cm^2s^{-1} – although with orders of magnitude uncertainty – for hydrogen has been extrapolated based on a wide range of accessible data measured at elevated temperatures [24]. This means that in our experiments the migration of hydrogen on a longer time scale cannot be excluded, however, vacancies seems to be more mobile, as for H a diffusion length of $(D_Ht)^{1/2}$ ~2.9 µm can be estimated for t = 24 hours duration. Considering all above, we conclude that the identification of the key mechanism responsible for the long term decay of the PMR signal in Fig. 4 requires further investigation that is beyond the scope of this work.

D. RESULTS OF PL MEASUREMENTS

Fig. 6 shows band-to-band (B2B) PL En-Vision line scan measurement performed along lateral direction through the stripes implanted with 1.5 MeV protons to five different doses in the range 10^{11}-10^{15} H^+cm^{-2}. Despite the very low
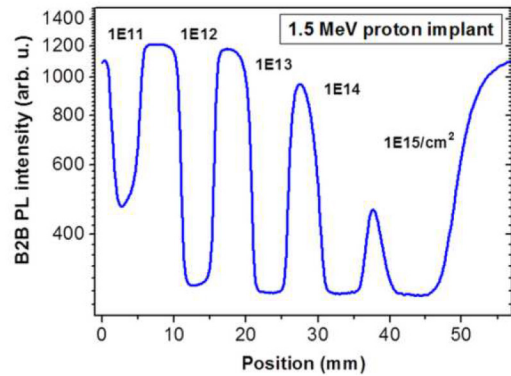

FIGURE 6. Band-to-band PL emission line scan performed through the stripes implanted with 1.5 MeV protons to different doses.

defect concentrations, the PL intensity in the implanted zones is strikingly lower compared to that of bare Si (PL signal level at a position of about 7.5 mm, in between the lowest dose implanted stripes in Fig. 6). This can be attributed to the fact that the implanted region penetrates deep into the material hence the total amount of defects and related free carrier recombination centers is significant within the full penetration range of the exciting laser beam. The PL intensity drops strikingly already for the lowest dose, decreases further for 10^{12} H^+cm^{-2}, and at higher doses seems to be saturated at around a minimum background level. This trend can be elucidated considering the effective depth accessible for the generated carriers $d_{eff} = \alpha^{-1}+(D\tau_{tot})^{1/2}$, where α is light absorption depth for the exciting laser beam (at λ = 808 nm) and $(D\tau_{tot})^{1/2}$ gives diffusive dispersion of excess carriers within their lifetime period (τ_{tot}) related endurance before recombination. In bare Si the estimated order of d_{eff} is ~80 µm while for a dose of 10^{13} H^+cm^{-2} d_{eff} drops to about ~30 µm that is about the implanted layer thickness, d_{imp}. For higher doses d_{eff} decreases further and fast defect related recombination of excess carriers may dominate over band-to-band recombination. Also, in this case crystalline substrate related B2B PL contribution no longer can be expected. This may be reflected in the saturation of the B2B PL intensity at a minimum background level. Nevertheless, the PL intensity seems to be very sensitive to the implanted dose in the low dose region below 10^{13} H^+cm^{-2}.

Worth to mention that in this work the noise level for the PMR signal can be somewhat higher for this unique experiment set as compared to high-throughput industrial implantation runs which are performed with two dimensional beam scans on full-wafer scale and are probed with PMR on a given number of measurement sites. In such case, the high spatial resolution of the PMR tool can be also applied for preparing sample homogeneity maps. In those applications, repeatability and dose sensitivity of PMR can be even further improved. Nevertheless, PMR's figures of merit are progressively enhanced thanks to the continuous development of the tool.

IV. CONCLUSION

We have shown that PMR-3000S can well resolve the differences in implanted dose, even at very low damage levels in the ppb-ppm range, and also capable to monitor time dependent processes related to long term defect structure changes in high-energy hydrogen implanted layers. This is thanks to the high sensitivity of the technique to concentration and lifetime changes of generated excess carriers that is caused by tiny differences in the dilute defect structure. In addition to low dose monitoring capability, applying a simplified evaluation procedure, PMR seems to be suitable to follow defect accumulation kinetics in proton implanted samples at low defect levels.

PMR based high-sensitivity characterization of both the short and long-term behavior of dilute defect structures may be beneficial in industrial process timing and post-implantation monitoring of high energy H^+ implanted wafers.

REFERENCES

[1] P. Hazdra, K. Brand, J. Rubes, and J. Vobecky, "Local lifetime control by light ion irradiation: Impact on blocking capability of power P-i-N diode," *Microelectron. J.*, vol. 32, no. 5, pp. 449–456, 2001.

[2] A. Hallen, M. Bakowski, and M. Lundqvist, "Multiple proton energy irradiation for improved GTO thyristors," *Solid-State Electron.*, vol. 36, no. 2, pp. 133–141, 1993.

[3] Y. Zohta, Y. Ohmura, and M. Kanazawa, "Shallow donor state produced by proton bombardment of silicon," *J. Appl. Phys.*, vol. 10, no. 4, p. 532, 1971.

[4] F. Dortu, T. Clarysse, R. Loo, and W. Vandervorst, "Extracting active dopant profile information from carrier illumination power curves," *J. Vac. Sci. Technol. B, Microelectron. Nanometer Struct. Process. Meas. Phenomena*, vol. 24, p. 375, Jan. 2006.

[5] F. Dortu, T. Clarysse, R. Loo, B. Pawlak, R. Delhougne, and W. Vandervorst, "Progress in the physical modeling of carrier illumination," *J. Vac. Sci. Technol. B, Microelectron. Nanometer Struct. Process. Meas. Phenomena*, vol. 24, p. 1131, Apr. 2006.

[6] E. Gaubas *et al.*, "In situ analysis of the carrier lifetime in silicon during implantation of 1.5 MeV protons," *Lithuanian J. Phys.*, vol. 50, no. 4, pp. 427–433, 2010.

[7] T. Ceponis *et al.*, "In situ analysis of carrier lifetime and barrier capacitance variations in silicon during 1.5 MeV protons implantation," *J. Instrum.*, vol. 6, Sep. 2011, Art. no. P09002.

[8] J. Szívós *et al.*, "Dose monitoring in MeV energy hydrogen implanted silicon by photo-modulated reflectance measurements," in *Proc. 20th Int. Workshop Junction Technol.*, Jun. 2021, pp. 1–3.

[9] I. Rajta *et al.*, "Accelerator characterization of the new ion beam facility at MTA Atomki in Debrecen, Hungary," *Nucl. Instr. Meth. Phys. Res. A, Accelerators Spectrometers Detect. Assoc. Equip.*, vol. 880, pp. 125–130, Feb. 2018.

[10] J. F. Ziegler, J. P. Biersack, and U. Littmark, *The Stopping and Range of Ions in Solids*. New York, NY, USA: Pergamon Press, 1985.

[11] M. Posselt, B. Schmidt, C. S. Murthy, T. Feudel, and K. Suzuki, "Modeling of damage accumulation during ion implantation into single-crystalline silicon," *J. Electrochem. Soc.*, vol. 144, no. 4, p. 1495, 1997.

[12] F. Dortu, "Low frequency modulated optical reflectance for the one-dimensional characterization of ultra shallow junctions (lage frequentie gemoduleerde optische reflectie voor de eendimensionale karakterisatie van ultra dunne juncties)," Ph.D. dissertation, Dept. Electr. Eng. ESAT, IMEC, Leuven, Belgium, 2009.

[13] J. Bogdanowicz *et al.*, "Advances in optical carrier profiling through high-frequency modulated optical reflectance," *J. Vac. Sci. Technol. B, Microelectron. Nanometer Struct. Process. Meas. Phenomena*, vol. 26, p. 310, Jan. 2008.

[14] M.-L. David, E. Oliviero, C. Blanchard, and J. F. Barbot, "Generation of defects induced by MeV proton implantation in silicon—Influence of nuclear losses," *Nucl. Instr. Meth. Phys. Res. B, Beam Interactions Mater. Atoms* vol. 186, pp. 309–312, Jan. 2002.

[15] I. Capan, Z. Pastuovic, R. Siegele, and R. Jaćimović, "Vacancy-related defects in n-type Si implanted with a rarefied microbeam of accelerated heavy ions in the MeV range," *Nucl. Instr. Meth. Phys. Res. B, Beam Interactions Mater. Atoms*, vol. 372, pp. 156–160, Apr. 2016.

[16] C. Nyamhere, "Characterization of process and radiation induced defects in Si and Ge using conventional deep level transient spectroscopy (DLTS) and Laplace-DLTS," Ph.D. dissertation, Faculty Nat. Agr. Sci., Univ. Pretoria, Pretoria, South Africa, 2019.

[17] G. Jellison and F. Modine, "Optical functions of silicon at elevated temperatures," *J. Appl. Phys.*, vol. 76, no. 6, p. 3758, 1994.

[18] F. Ujhelyi *et al.*, "Mid-low energy implantation tilt angle monitoring with photomodulated reflectance measurement," in *Proc. 30th Annu. SEMI Adv. Semicond. Manuf. Conf. (ASMC)*, Saratoga Springs, NY, USA, May 2019, pp. 1–4.

[19] A. Pongrácz *et al.*, "Tilt angle and dose rate monitoring of low energy ion implantation processes with photomodulated reflectance measurement," in *Proc. 31st Annu. SEMI Adv. Semicond. Manuf. Conf. (ASMC)*, Saratoga Springs, NY, USA, Aug. 2020, pp. 1–4.

[20] Z. Zolnai *et al.*, "Room temperature micro-photoluminescence measurements for monitoring defects in low-energy high-dose As and B implanted silicon," in *Proc. 32st Annu. SEMI Adv. Semicond. Manuf. Conf. (ASMC)*, May 2021, pp. 1–6.

[21] G. D. Watkins, "The vacancy in silicon: Identical diffusion properties at cryogenic and elevated temperatures," *J. Appl. Phys.*, vol. 103, no. 10, 2008, Art. no. 106106.

[22] V. V. Voronkov and R. Falster, "The diffusivity of the vacancy in silicon: Is it fast or slow?" *Mater. Sci. Semicond. Process.*, vol. 15, pp. 697–702, Dec. 2012.

[23] K. L. Wang, Y. H. Lee, and J. W. Corbett, "Defect distribution near the surface of electron-irradiated silicon," *Appl. Phys. Lett.*, vol. 33, no. 6, p. 547, 1978.

[24] M. Faccinelli *et al.*, "Diffusion of hydrogen in proton implanted silicon: Dependence on the hydrogen concentration," 2016, *arXiv:1611.04312*.